ACS Photonics

Article

pubs.acs.org/journal/apchd5

Low-Threshold near-Infrared GaAs–AlGaAs Core–Shell Nanowire Plasmon Laser

Jinfa Ho,* Jun Tatebayashi, Sylvain Sergent, Chee Fai Fong, Satoshi Iwamoto, and Yasuhiko Arakawa*

Institute for Nano Quantum Information Electronics, The University of Tokyo, 4-6-1 Komaba, Meguro-ku, Tokyo 153-8505, Japan

Supporting Information

ABSTRACT: We demonstrate plasmonic lasing from metal–organic chemical vapor deposition (MOCVD)-grown GaAs–AlGaAs core–shell nanowires (NWs) with subdiffraction limit diameters of ∼150 nm placed directly on a silver thin film. The absence of a low-index dielectric spacer layer between the NW and the metal layer allows for surface plasmon polariton (SPP) lasing using a nonhybridized plasmonic mode. Unlike previously reported plasmonic NW lasers using the fundamental SPP mode, we demonstrate for the first time plasmonic NW lasing under pulsed optical excitation by using the higher order SPP mode. The higher order mode allows us to alleviate the high losses associated with the fundamental plasmonic mode. We observed lasing at temperatures up to 125 K. Our demonstration of a plasmonic laser based on GaAs emitting in the near-infrared region will be useful for the on-chip integration of nanophotonic and electronic devices and the development of GaAs-based plasmonic devices.

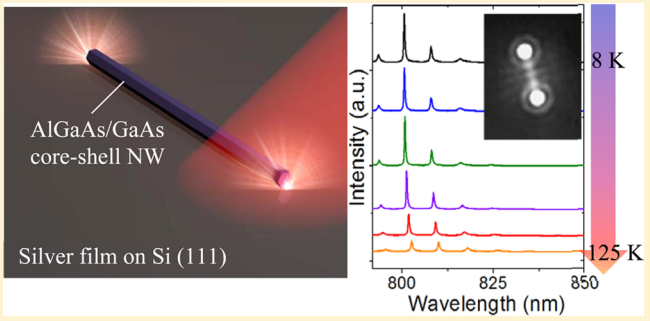

KEYWORDS: *nanowire, surface plasmon polariton laser, GaAs plasmonics, subdiffraction limit optics*

The nanolaser is a key component for the on-chip integration of nanophotonics and electronics with ultralow power consumption.[1,2] Compared to other laser structures, semiconductor nanowires (NWs) are well suited for the miniaturization of lasers, as the large refractive index of semiconductors and the wire-like geometry enables strong two-dimensional confinement of optical modes guided along the NW axis. The end facets provide optical feedback for Fabry–Pérot modes in the longitudinal direction and also lasing output via scattering. In addition, by placing NWs on a metallic surface, surface plasmon polariton (SPP) modes[3,4] can be supported, enabling lasing at subdiffraction limit dimensions. NW plasmonic lasers emitting in the visible range based on ZnO,[5] GaN,[6] InGaN,[7−9] and CdS[10] have already been demonstrated. However, lasing from GaAs NWs in the technologically important near-infrared region has so far been limited to dielectric optical cavities,[11,12] which are impeded by the diffraction limit. The development of plasmonic devices based on GaAs has been hampered by the large losses of SPP modes at a GaAs–metal interface;[13] this is further compounded by the large nonradiative surface recombination rates[14,15] and long carrier diffusion length of GaAs.[16] Indeed, while there have been a few reports of plasmonic lasers in the near-infrared based on InP using a nanopan structure[17] and InGaAlAs using a ridge structure,[18] there have been no reports on plasmonic NW lasers based on GaAs. Here, we demonstrate plasmonic lasing with GaAs/AlGaAs core–shell NWs with diameters of ∼150 nm placed directly on a silver film under pulsed excitation conditions. While there have been reports of plasmonic lasers with the semiconductor in direct contact with the metal,[17] plasmonic NW lasers to date have achieved lasing by using a hybridized plasmon-waveguide mode confined in a thin low-index dielectric layer sandwiched between the NW and the metal surface to alleviate high losses associated with the nonhybridized plasmonic mode.[5−10] By placing our NWs in direct contact with the silver film, we observe lasing from the nonhybridized plasmonic mode. Lasing in our structure was achieved by using the low-loss higher order SPP mode, which requires a relatively large contact area between the NW and the silver substrate. Despite larger propagation losses compared to hybridized plasmon-waveguide modes, the higher order SPP mode exhibits superior mode confinement to the NW core region, and lower lasing thresholds may be achieved with the higher order SPP mode (see Supporting Information). The detrimental effects of scattering losses, high ohmic losses, and nonradiative surface recombination are suppressed by using a smooth, single-crystalline silver film and AlGaAs capping of the GaAs gain core.

RESULTS AND DISCUSSION

Sample Preparation of GaAs–AlGaAs Core–Shell NW Plasmonic Lasers on an Ordered Silver Film. The NWs used in this study were grown by selective area metal–organic chemical vapor deposition (MOCVD) on GaAs(111) B substrates (see Methods section). The grown NWs have

Received: October 24, 2014
Published: December 10, 2014

DOI: 10.1021/ph5003945
ACS Photonics 2015, 2, 165−171

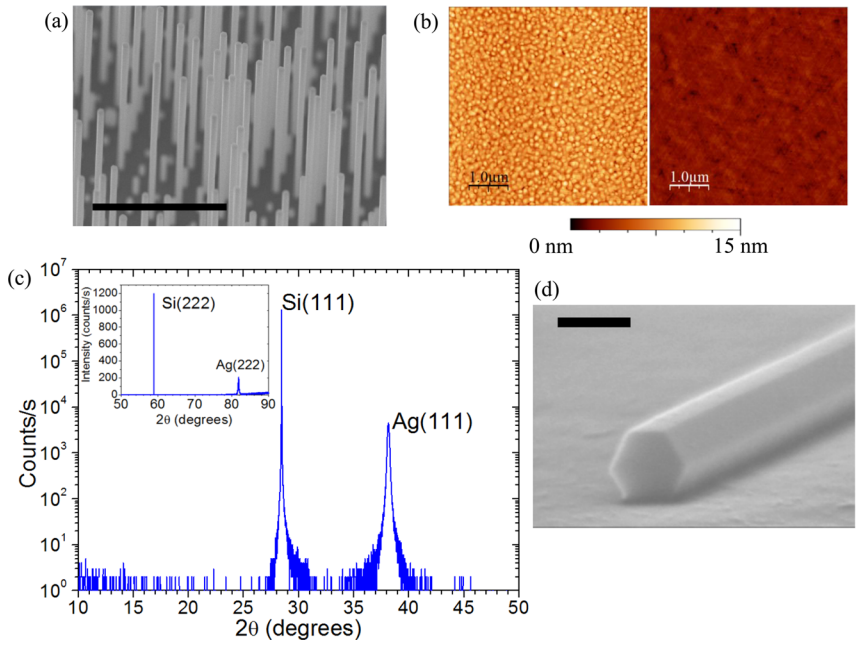

Figure 1. (a) Scanning electron microscopy (SEM) image showing the as-grown GaAs/AlGaAs core−shell NWs. Scale bar is 3 μm. (b) AFM images of the as-deposited silver film (left panel) with rms roughness of ∼1.4 nm and the silver film after annealing at 550 °C for 5 min (right panel) with rms roughness of ∼0.4 nm. (c) XRD pattern of silver film on silicon substrate after annealing. The silver film has a (111) single-crystalline structure. Inset shows extended XRD pattern, showing only second-order peaks from Si(111) and Ag(111). Additional peaks arising from Ag_xO are also absent, indicating that the film has not been oxidized from the high-temperature annealing process. (d) SEM image of NW dispersed on silver, showing good contact between the NW and silver. Scale bar is 150 nm.

varying heights and untapered diameters of ∼150 nm, which includes a layer of $Al_{0.1}Ga_{0.9}As$ with a ∼5 nm thickness estimated from the growth conditions. Figure 1a shows a typical scanning electron microscopy image of the as-grown core−shell NWs. The MOCVD-grown GaAs NWs exhibit low surface roughness, and we place them directly on the silver film, so the contact is limited by the silver film roughness. To reduce propagation losses of the plasmonic mode due to scattering, it is important to fabricate a smooth, single-crystalline silver film with suppressed surface roughness and grain boundaries. While previous reports using a crystalline film[7,9] require an elaborate molecular beam epitaxy growth method, we describe here a much simpler fabrication process that can achieve a comparable silver film quality. We grow a thin silver film (thickness of 150 nm) by electron-beam evaporation of a silver target onto a Si(111) substrate at a rate of 0.5 Å/s under a low pressure of 3.0×10^{-5} Pa at room temperature. The as-deposited silver film has a large root-mean-square (rms) surface roughness of ∼1.4 nm, and we perform annealing at 550 °C for 5 min in an N_2 environment to reduce the roughness down to ∼0.4 nm, as shown in the atomic force microscopy (AFM) images in Figure 1b. Due to coincident lattice site matching between the silver and Si(111) lattice sites, the silver film also acquires a single-crystalline (111) structure.[19,20] This can be seen in the X-ray diffraction (XRD) pattern in Figure 1c, which shows only peaks from Si(111), Ag(111), and their respective second-order peaks (inset, Figure 1c). Peaks arising from Ag_xO are also notably absent from the XRD pattern, indicating that oxidation of the silver film does not occur from the high-temperature annealing process.

To disperse the NWs laterally on silver, we break the as-grown NWs in an isopropyl alcohol solution via ultrasonication and transfer them to the silver film using a drop-casting method. Figure 1d shows a typical scanning electron microscopy image of a NW dispersed on silver, showing that good contact between the NW and silver is achieved. This, together with a uniform NW diameter, is necessary to ensure that SPP modes are supported uniformly along the NW. While previous reports on NW plasmonic lasers insert a low-index dielectric layer between the NW and the metal to reduce propagation losses and prevent nonradiative quenching,[5−10] we place our NWs in direct contact with the silver layer, with the AlGaAs shell preventing nonradiative quenching at the silver interface. Due to direct contact between the NW and silver, the supported mode is no longer concentrated in the low-index dielectric layer, and it is possible to have a better mode penetration and overlap with the gain region of the NW (see Supporting Information). This can be useful in applications where strong coupling between the plasmonic mode and quantum wells/dots embedded in the NW is desired.

Spectroscopy of GaAs−AlGaAs NW Plasmonic Lasers. The optical properties of the NWs were measured using microphotoluminescence (μ-PL) spectroscopy. The samples containing well-dispersed NWs were placed in a He-flow variable-temperature cryostat and optically excited with a pulsed semiconductor diode laser (PicoQuant) with an emission peak at 785 nm, a ∼50 ps pulse duration, and a 5 MHz repetition frequency (duty cycle $\sim 2.5 \times 10^{-4}$). An objective lens (50×, NA = 0.65) was used to focus the laser beam down to a spot with a diameter of ∼2 μm, and the NW emission is collected through the same lens. The emission of the NWs is strongest at the end facets where scattering occurs, as can be seen in Figure 2a, insets. The beam spot is smaller than the NW length and was focused on one of the NW end facets to maximize the collection efficiency of the NW emission. The spectrometer slit was adjusted to spatially filter the detection area laterally to a ∼1 μm range, which was then dispersed by a 300 mm^{-1} grating in a 75 cm spectrometer,

DOI: 10.1021/ph5003945
ACS Photonics 2015, 2, 165−171

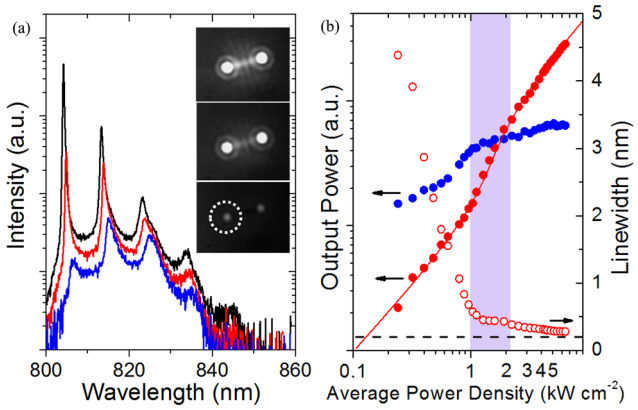

Figure 2. (a) Emission spectra for a NW with a diameter of 150 nm and length of 4.77 μm at three power densities showing the transition of the mode at 804 nm from spontaneous emission at 0.4 kW/cm^2 (blue) to amplified spontaneous emission at 1.3 kW/cm^2 (red) and to lasing at 4.8 kW/cm^2 (black). Note the logarithmic scaling of the intensity axis. The insets show optical microscope images of the NWs at spontaneous emission (bottom), amplified spontaneous emission (middle), and lasing (top). The white dotted circle is the approximate pump laser excitation and collection area. (b) Double logarithmic $L-L$ plot of lasing peak at 804 nm (solid red circles) and corresponding line width narrowing behavior (open red circles). The black dotted line is the line width resolution limit of our optical setup. The purple-shaded area is the region of amplified spontaneous emission, and the lasing threshold is at ~1.0 kW/cm^2. The spontaneous emission output (solid blue circles), plotted on the same scale as the lasing output power, is extracted from the background Gaussian emission and is clamped beyond the threshold.

giving a spectral resolution limit of 0.2 nm, before being detected with a charge coupled device camera. A separate charge coupled device camera was used to image the sample, providing sufficient resolution for the length but not the diameter of each individual NW to be measured.

We first perform μ-PL at 8 K on NWs with diameters of ~150 nm and an average length of ~5 μm dispersed on SiO_2 to investigate the emission properties of our NWs without plasmonic effects. A diameter of ~150 nm is below the diffraction limit for GaAs emission wavelengths.[21,22] The emission spectra for a typical NW show a featureless, broad Gaussian-like emission for all pump powers (see Supporting Information, Figure S1), indicating that, as expected, NWs with diameters 150 nm and below do not support Fabry–Pérot modes for photonic modes. At a low average excitation power of 0.8 kW/cm^2, the GaAs emission is centered at 830 nm, which is red-shifted from the expected bulk zinc-blende GaAs emission peak of 819 nm.[23,24] This can be explained by the presence of zinc-blende/wurtzite heterostructure in the NWs, where spatially indirect recombination occurs between electrons confined in the zinc-blende phase and holes trapped in the wurtzite phase at the zinc-blende/wurtzite interface. This lowers the transition energy and causes the red-shift of the GaAs emission peak. In addition, spatially direct recombination in the zinc-blende and wurtzite regions also occurs, resulting in inhomogeneous broadening,[23,25] which accounts for the comparatively large bandwidth of the GaAs emission. We also observe a blue-shift of the peak intensity wavelength with increasing excitation powers due to the band filling effect. Furthermore, we investigated the luminescence of NWs without AlGaAs capping and observed poor emission properties due to nonradiative surface recombination.[14,15] This is similar to previous studies[11,12,26,27] on GaAs NWs and highlights the importance of the AlGaAs capping to ensure a good optical yield.

Next, we performed μ-PL on similar NWs dispersed on silver. Typical power-dependent spectra for a NW with a diameter of ~150 nm and a length of ~5 μm are shown in Figure 2a with accompanying microscope images of the NW emission. In contrast with NWs dispersed on SiO_2 (see Supporting Information), regularly spaced longitudinal Fabry–Pérot mode peaks can be seen at 804, 813, 823, and 834 nm. Above an average pump power density of ~1.0 kW/cm^2, the peak at 804 nm increases sharply in intensity and its line width narrows, which is a signature of lasing. The microscope images also provide evidence for plasmonic lasing; unlike optical modes, SPP modes are tightly confined to the metal–dielectric interface and do not radiate to the far-field until they are scattered from the end facets of the NWs.[7,28] It is clearly seen in the inset of Figure 2a that the NW bulk is only weakly luminescent and the main emission is coming from the NW end facets, in contrast to reports on photonic NW lasers that show strong emission from the entire NW bulk[12,29] especially below threshold. Above threshold, clear interference fringes can also be observed, which is indicative of coherent radiation generated in the NW cavity.[29] It is also noteworthy that we are able to use a focused beam spot (~2 μm in diameter) that is smaller than the NW to create population inversion throughout the NW. This can be attributed to the long carrier diffusion length in AlGaAs-capped GaAs NWs.[13] We have verified that lasing behavior can be observed regardless of excitation location along the NW length. Further reduction in the lasing threshold can be expected with homogeneous pumping of the NWs by using a cylindrical lens to create an elliptical beam spot, which can reduce material loss from the unpumped regions of the NWs. The light input–light output ($L-L$) plot of the lasing peak at 804 nm is shown in Figure 2b and exhibits a nonlinear S-shape, with the concurrent onset of the line width narrowing plateau and the nonlinear kink at ~1.0 kW/cm^2 being an indication of lasing behavior. On the basis of a simple rate equation fitting model[10,30] (see Methods section), the carrier density at threshold is ~2.4×10^{18} cm^{-3} and a spontaneous emission coupling β factor larger than 0.2 was obtained. The other Fabry–Pérot modes are nonlasing and show a sublinear increase with pump power.

Compared with previous reports on photonic GaAs NW lasers,[11,12] the threshold (after conversion to joules cm^{-2}/pulse) of our NW laser is at least 1 order of magnitude smaller at 8 K and is promising for high-temperature lasing. We investigated the high-temperature performance of a NW with a diameter of ~150 nm and a length of ~6.0 μm. The temperature-dependent $L-L$ plots of the main lasing peak near 800 nm, along with the corresponding line width narrowing behavior, are shown in Figure 3a. We observed lasing behavior up to 125 K. At 150 K, we could observe amplified spontaneous emission apparent from the superlinear kink at ~5.0 kW/cm^2, but lasing was not achieved at the maximum pump power of our laser. The emission spectra at a high average pump power of 5.7 kW/cm^2 from 8 to 150 K are shown in Figure 3b. The decrease of the peak intensity of the main lasing peak with increasing temperature suggests gain reduction induced by higher temperatures.[31] While only the mode at 800 nm is lasing at 8 K, multimode lasing is observed above 100 K, with the peak at 810 nm also showing an S-shaped $L-L$ dependence (Supporting Information Figure S3).

DOI: 10.1021/ph5003945
ACS Photonics 2015, 2, 165–171

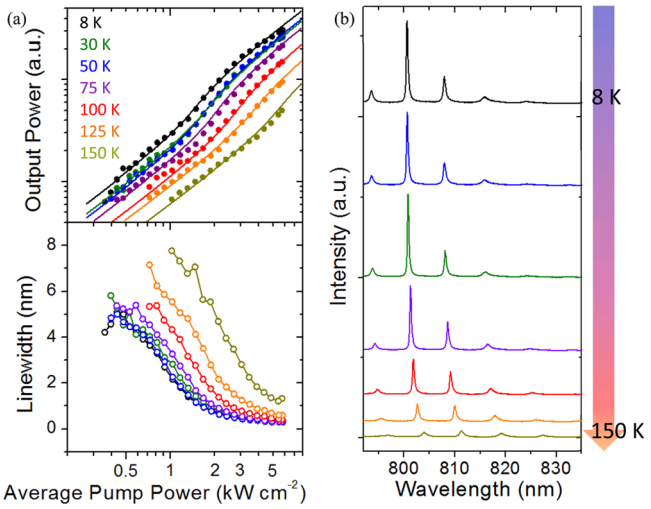

Figure 3. (a) L–L plots (top) with accompanying line widths (bottom) of the peak at ∼800 nm for a NW with diameter ∼150 nm and length of 6.0 μm at 8 K (black), 30 K (green), 50 K (blue), 75 K (purple), 100 K (red), 125 K (orange), and 150 K (olive). (b) Temperature-dependent spectra of NW at 5.7 kW/cm^2.

This suggests that the gain bandwidth has broadened to levels comparable to the peak spacing. The red-shift of the Fabry–Pérot peak positions is due to the refractive index change of GaAs at higher temperatures.

Numerical Analysis of Experimental Results. To clarify the nature of the lasing plasmonic mode, we performed 2D finite-difference eigenmode[32] simulations (see Methods section) to determine the field distributions of the modes supported by the NW laser and their losses. Simulations for GaAs NWs with diameters smaller than 200 nm on a SiO_2 substrate show that no photonic modes are supported, which is in agreement with μ-PL experiments performed on NWs dispersed on SiO_2. In contrast, the same NWs placed on silver can support two distinct SPP modes with field distributions shown in Figure 4a together with their propagation losses and their real part of the effective indices as a function of the NW diameter. The fundamental mode exists for NWs of all diameters we investigated and exhibits large losses and high confinement to the NW/silver interface. This is similar to the lasing mode observed in previous reports of plasmonic NW lasers.[5−10] However, we find that a higher order SPP mode with lower losses is also supported by NWs with diameters larger than 140 nm. The lower losses can be explained by the poorer confinement of the higher order mode to the lossy GaAs/silver interface, enabling a significant portion of the mode energy to be stored in the nonmetallic regions, and the smaller group index of the higher order mode. The group index n_g is calculated by

$$n_g = \frac{\lambda^2}{2\Delta\lambda L} \tag{1}$$

from Figure 4b. The higher order mode has a smaller n_g of ∼6 compared to the fundamental mode group index with an n_g of ∼9. Due to the lower losses, the higher order mode is more likely to lase. This mode requires a relatively large contact region between the NW and silver and is thus not supported by smaller NWs and NWs with circular cross-sections. The expected mode spacing for each mode can be calculated by

$$\Delta\lambda = \left(\frac{\lambda^2}{2L}\right)\left(n_{\mathrm{eff}} - \lambda\frac{\mathrm{d}n_{\mathrm{eff}}}{\mathrm{d}\lambda}\right)^{-1} \tag{2}$$

where n_{eff} is the effective mode index of a longitudinal guided mode in a NW with length L, and $\mathrm{d}n_{\mathrm{eff}}/\mathrm{d}\lambda$ is the dispersion relation of the mode. The calculated mode spacing for both SPP modes is shown in Figure 4b as a function of $1/L$, and our experimentally observed mode spacing corresponds well to that of the higher order mode.

While the fundamental mode should exist for all NW diameters, we do not observe it for NWs with diameters of 150 nm dispersed on silver. This could be due to the large propagation losses of the fundamental mode. To confirm the presence of the fundamental mode, we performed μ-PL experiments on NWs with diameters of ∼90 nm dispersed on silver. This is below the cut-off diameter for the higher order mode, and only the fundamental SPP mode is supported. Typical power-dependent spectra are shown in Figure 5a. While regularly spaced Fabry–Pérot modes are visible, the line widths are much larger due to the higher losses of the

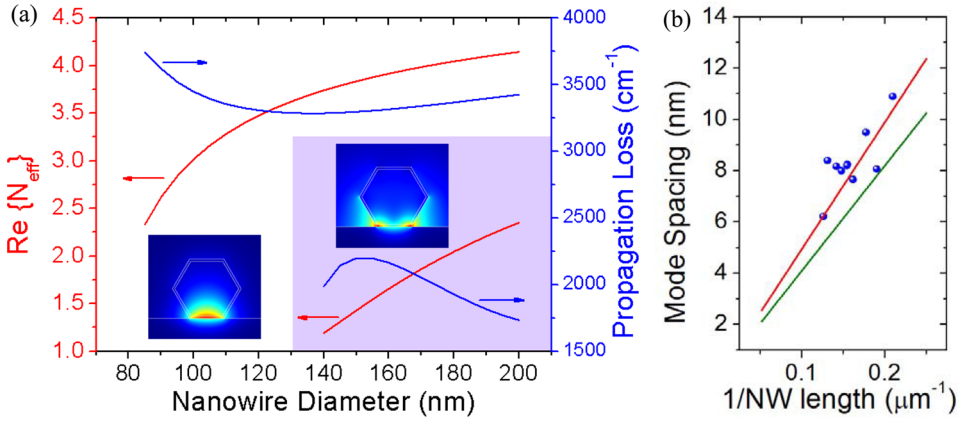

Figure 4. (a) Calculated real part of effective index (red curves) and propagation losses (blue curves) for the fundamental SPP mode and higher order SPP mode (purple-shaded region) as a function of the NW diameter. Insets show the field distributions for the fundamental mode and the higher order mode (purple-shaded region) for a NW with 150 nm diameter. (b) Calculated mode spacing as a function of $1/L$ for the fundamental SPP mode (green line) and the higher order mode (red line). The experimentally observed mode spacing for NWs with diameter ∼150 nm is shown by the blue dots and corresponds well to the calculated higher order mode spacing.

DOI: 10.1021/ph5003945
ACS Photonics 2015, 2, 165−171

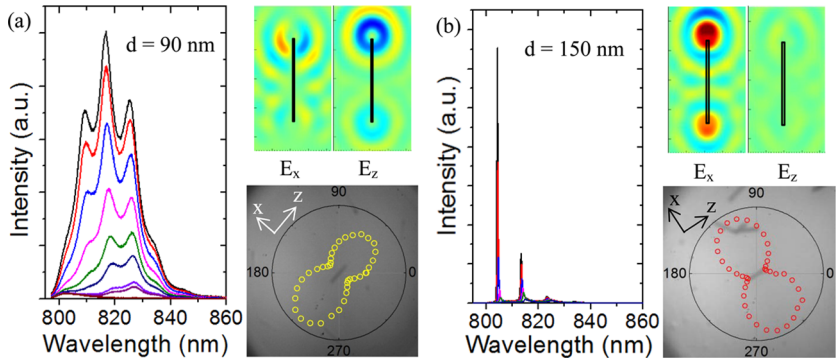

Figure 5. (a) Power-dependent spectra from 0.1−7.0 kW/cm^2 for a NW with diameter ∼90 nm dispersed on silver. The Fabry−Pérot modes observed are from the fundamental SPP mode and have the same polarization. The polarization for the peak at ∼815 nm is shown superimposed on the NW image. The scattered E_x and E_z fields of the fundamental mode obtained by FDTD simulations are shown (plotted on the same scale for comparison), with the position of the NW outlined in black. The relative intensities of the E_x and E_z fields agree well with the observed polarization. (b) Similar experiments and FDTD simulations were performed for a NW with diameter ∼150 nm. Fabry−Pérot peaks observed come from the higher order SPP mode and are polarized perpendicular to the NW long axis (x-direction). Polarization dependence for the peak at 804 nm is shown superimposed on the NW image and agrees well with the relative E_x and E_z intensities obtained from FDTD calculations.

fundamental mode. As a result, we were not able to achieve lasing with the fundamental SPP mode. Furthermore, we measured the polarization dependence of the fundamental mode emission (Figure 5a) and find that all the modes are polarized parallel to the NW long axis. In contrast, the modes are polarized perpendicular to the NW axis for NWs with diameters of ∼150 nm, which support the higher order mode (Figure 5b). The difference in polarization of the modes was verified by our finite-difference time-domain (FDTD) simulations (see Methods section), performed for NWs with diameters of 90 and 150 nm. The fundamental mode and higher order mode were launched in the direction of the NW long axis (z-direction) from the middle of 5 μm long NWs. The scattered E_x and E_z fields from the NW end facets are shown in Figure 5a and b, and the asymmetric field distribution in the z-direction is due to propagation losses along the NW. The relative intensities of E_x and E_z agree well with the measured polarizations, and we conclude that the observed lasing mode is indeed the higher order SPP mode. It is likely that the relatively high temperature plasmonic lasing in our NWs was made possible by lower propagation losses of the higher order SPP mode. Nevertheless, it remains challenging to achieve lasing at room temperature with our NW laser design, and the incorporation of quantum wells or quantum dots,[33] which can provide higher optical gain at high temperatures due to an increased density of states, may be required. Indeed, room-temperature plasmonic lasing at continuous wave pumping has already been observed for nanorod structures using InGaN/GaN multiple quantum wells as a gain medium.[8] Quantum well/dot structures in GaAs systems are usually formed by using InGaAs, which is also promising for extending the lasing wavelength closer toward the telecommunications window.

CONCLUSION

We have demonstrated a nanowire plasmonic laser based on the GaAs−AlGaAs core−shell structure and observed lasing at up to 125 K. Lasing with a low threshold of 1.0 kW/cm^2 at 8 K was achieved with the higher order plasmonic mode. The use of a silicon (111) substrate to create a smooth, single-crystalline silver film using a simple fabrication method also allows for integration with silicon processes. This is the first demonstration of a plasmon NW laser based on GaAs emitting in the near-infrared region and will be useful for nanophotonic−electronic integration applications and the development of GaAs-based plasmonic devices.

METHODS

Growth of Core−Shell GaAs/AlGaAs NWs. The GaAs/AlGaAs core−shell NWs were grown using selective area metal−organic chemical vapor deposition on GaAs(111) B substrates. A 15 nm SiO_2 layer was sputtered onto the substrate surface, and a two-dimensional array of apertures (pitch = 250 nm, diameter = 44.8 ± 1.3 nm) where GaAs NW growth occurs was created using standard electron-beam lithography technique followed by reactive ion etching. The GaAs core was grown at a temperature of 750 °C with a V/III ratio of 600. A layer of $Al_{0.1}Ga_{0.9}As$ was then grown (with a V/III ratio of 50) around the core to form a shell of ∼5 nm thickness, estimated from the growth conditions. Finally, the structure was capped with a thin layer of GaAs to prevent oxidation of the Al content in the AlGaAs shell.

Numerical Simulations. 2-D finite difference frequency domain and 3-D FDTD simulations were performed with Lumerical MODE Solutions and FDTD Solutions, respectively. The cross-sectional mode distributions were obtained with 2-D FDFD simulations. The scattered electric field was obtained using FDTD simulations by launching the mode distributions obtained from the 2-D FDFD simulations in a 3-D geometry. For all our simulations, we used a hexagonal GaAs−AlGaAs core−shell NW geometry, placed directly on silver. Regardless of the NW diameter, we assumed an AlGaAs shell thickness of 5 nm. For an operational wavelength of 800 nm, the refractive indices are n_{AlGaAs} = 3.62[34] and n_{GaAs} = 3.66, and the material properties of silver were obtained from ref 35.

Rate Equation Fitting. We have used a simple rate equation analysis model based on refs 10 and 30, given by

$$\frac{dn}{dt} = \sigma p(t) - A_{tot}n - \zeta A_{cav}s(n - n_0) - \Gamma n \quad (3)$$

$$\frac{ds}{dt} = \beta A_{tot}n + \zeta A_{cav}s(n - n_0) - \gamma_{ph}s \quad (4)$$

where n is the carrier number, s is the photon number, and n_0 is the carrier number at transparency, which we set to volume$_{NW}$ × 2.0 × 10^{18} cm^{-3}.[9] $p(t) = p_0 \exp(-((t - t_0)^2/\Delta t^2))$ is the

DOI: 10.1021/ph5003945
ACS Photonics 2015, 2, 165−171

incident pulsed pump laser, and we define the pulse width Δt to be 50 ps. σ is the pump laser photon to smiconductor carrier conversion efficiency. We assume that the total carrier decay rate $A_{tot} \approx A_{cav} + A_0$, where $A_{cav} = FA_0$ is the carrier decay rate into the cavity mode, and A_0 is the carrier decay rate into free space modes. We assumed A_0 is equal to the carrier decay rate in bulk GaAs = $(1\ \text{ns})^{-1}$. The Purcell factor F is calculated using Comsol's mode solver as outlined in ref 10. We obtain $F \approx 1$ for the higher order SPP mode. The mode overlap with the gain medium $\zeta \approx 0.4$ was obtained from finite difference eigenmode simulations (see Supporting Information, Figure S2). The main fitting parameters are the photon decay rate in the cavity (γ_{ph}) and the spontaneous emission coupling factor β. Typical β values we obtain from fitting to our results are ~0.2−0.4. The photon lifetime can be calculated from $\gamma_{ph} = \alpha_T \nu$ where ν is the group velocity of the mode and total loss $\alpha_T = \alpha - (1/L)\ \ln(R_1R_2)$ for a Fabry−Perot cavity. α is the propagation losses calculated in Figure 4a. The reflectivities of the NW facets are likely to differ largely from sample to sample as we break our NWs using ultrasonication, which results in facets that are not cleanly cleaved. On the basis of this fitting, our samples have reflectivities ranging from 0.1 to 0.36. The spontaneous emission coupling factor β and the nonradiative recombination rate Γ affect the transition at lasing threshold, with a small β and large Γ resulting in a more pronounced kink. There are no reports on the nonradiative recombination rate for systems similar to what we have studied, and this was set to 0 in our fitting. We justify this by the virtue of the AlGaAs capping of our NWs, but in reality some amount of nonradiative recombination is present due to the proximity of the silver film, and the fitting procedure gives us the lower bound of the β factor in this model. Our model assumes a single lasing mode and is valid for our experiments at lower temperatures, where only one lasing mode is present, and is likely to be less accurate at higher temperatures, where multiple lasing modes may be present.

■ ASSOCIATED CONTENT

Supporting Information

Details of spectra of NWs dispersed on SiO_2, comparison of hybrid plasmonic-waveguide mode and the higher order plasmonic mode, and data for multimode lasing at 125 K. This material is available free of charge via the Internet at http://pubs.acs.org.

■ AUTHOR INFORMATION

Corresponding Authors

*E-mail: jinfaho@iis.u-tokyo.ac.jp.
*E-mail: arakawa@iis.u-tokyo.ac.jp.

Author Contributions

J.H. carried out the modeling and theoretical analysis. J.H. fabricated the silver film with assistance from S.S., and J.T. fabricated the NWs. J.H. carried out the microphotoluminescence experiments with assistance from C.F.F. and S.S. J.H. carried out analysis of the experimental results with assistance from S.S. and S.I. J.H. wrote the manuscript, with contributions from all authors. Y.A. supervised the entire project.

Notes

The authors declare no competing financial interest.

■ ACKNOWLEDGMENTS

This work was supported by the Project for Developing Innovation Systems of the Ministry of Education, Culture, Sports, Science and Technology (MEXT), Japan, by the Japan Society for the Promotion of Science (JSPS) through its Funding Program for World-Leading Innovation R&D on Science and Technology (FIRST Program), and by the New Energy and Industrial Technology Development Organization (NEDO). J.H. is supported by the Agency of Science, Technology and Research of Singapore. The authors thank Y. Ota for fruitful discussions.

■ REFERENCES

(1) Altug, H.; Englund, D.; Vučković, J. Ultrafast photonic crystal nanocavity laser. *Nat. Phys.* **2006**, *2*, 484.

(2) Hill, M. T.; Oei, Y.-S.; Smalbrugge, B.; Zhu, Y.; de Vries, T.; van Veldhoven, P. J.; van Otten, F. W. M.; Eijkemans, T. J.; Turkiewicz, J. P.; de Warrdt, H.; Geluk, E. J.; Kwon, S.-H.; Lee, Y.-H.; Nötzel, R.; Smit, M. K. Lasing in metallic-coated nanocavities. *Nat. Photonics* **2007**, *1*, 589.

(3) Maier, S. A.; Kik, P. G.; Atwater, H. A.; Meltzer, S.; Harel, E.; Koel, B. E.; Requicha, A. A. G. Local detection of electromagnetic energy transport below the diffraction limit in metal nanoparticle plasmon waveguides. *Nat. Mater.* **2003**, *2*, 229.

(4) Pile, D. F. P.; Ogawa, R.; Gramotnev, D. K.; Okamoto, T.; Haraguchi, M.; Fukui, M.; Matsuo, S. Theoretical and experimental investigation of strongly localized plasmons on triangular metal wedges for subwavelength waveguiding. *Appl. Phys. Lett.* **2005**, *87*, 061106.

(5) Sidiropoulos, T. P. H.; Röder, R.; Geburt, S.; Hess, O.; Maier, S. A.; Ronning, C.; Oulton, R. F. Ultrafast plasmonic nanowire lasers near the surface plasmon frequency *Nat. Phys.* **2014**, *10*, 1038/nphys3103.

(6) Zhang, Q.; Li, G.; Liu, X.; Qian, F.; Li, Y.; Sum, T. C.; Lieber, C. M.; Xiong, Q. A room temperature low-threshold ultraviolet plasmonic nanolaser. *Nat. Commun.* **2014**, *5*, 4953.

(7) Lu, Y.-J.; Kim, J.; Chen, H.-Y.; Wu, C.; Dabidian, N.; Sanders, C. E.; Wang, C.-Y.; Lu, M. Y.; Li, B.-H.; Qiu, X.; Chang, W.-H.; Chen, L.-J.; Shvets, G.; Shih, C.-K.; Gwo, S. Plasmonic nanolaser using epitaxially grown silver film. *Science* **2012**, *337*, 450.

(8) Hou, Y.; Renwick, P.; Liu, B.; Bai, J.; Wang, T. Room temperature plasmonic lasing in a continuous wave operation mode from an InGaN/GaN single nanorod with a low threshold. *Sci. Rep.* **2014**, *4*, 5014.

(9) Lu, Y.-J.; Wang, C.-Y.; Kim, J.; Chen, H.-Y.; Lu, M.-Y.; Chen, Y.-C.l; Chang, W.-H.; Chen, L.-J.; Stockman, M. I.; Shih, C.-K.; Gwo, S. All-color plasmonic nanolasers with ultralow thresholds: autotuning mechanism for single-mode lasing. *Nano Lett.* **2014**, *14*, 4381.

(10) Oulton, R. F.; Sorger, V. J.; Zentgraf, T.; Ma, R.-M.; Gladden, C.; Dai, L.; Bartal, G.; Zhang, X. Plasmon lasers at deep subwavelength scale. *Nature* **2009**, *461*, 629.

(11) Mayer, B.; Rudolph, D.; Schnell, J.; Morkötter, S.; Winner, J.; Treu, J.; Müller, K.; Bracher, G.; Abstreiter, G.; Koblmüller, G.; Finley, J. J. Lasing from individual GaAs-AlGaAs core-shell nanowires up to room temperature. *Nat. Commun.* **2013**, *4*, 2931.

(12) Saxena, D.; Mokkapati, S.; Parkinson, P.; Jiang, N.; Gao, Q.; Tan, H. H.; Jagadish, C. Optically pumped room-temperature GaAs nanowire lasers. *Nat. Photonics* **2013**, *7*, 963.

(13) Atwater, H. A.; Polman, A. Plasmonics for improved photovoltaic devices. *Nat. Mater.* **2010**, *9*, 205.

(14) Chang, C.-C.; Chi, C.-Y.; Yao, M.; Huang, N.; Chen, C.-C.; Theiss, J.; Bushmaker, A. W.; LaLumondiere, S.; Yeh, T.-W.; Povinelli, M. L.; Zhou, C.; Dapkus, P. D.; Cronin, S. B. Electrical and optical characterization of surface passivation in GaAs nanowires. *Nano Lett.* **2012**, *12*, 4484.

(15) Jiang, N.; Parkinson, P.; Gao, Q.; Breuer, S.; Tan, H. H.; Wong-Leung, J.; Jagadish, C. Long minority carrier lifetime in Au-catalyzed GaAs/$Al_xGa_{1-x}As$ core-shell nanowires. *Appl. Phys. Lett.* **2012**, *101*, 023111.

DOI: 10.1021/ph5003945
ACS Photonics 2015, 2, 165−171

(16) Bolinsson, J.; Mergenthaler, K.; Samuelson, L.; Gustafsson, A. Diffusion length measurements in axial and radial heterostructured nanowires using cathodoluminescence. *J. Cryst. Growth* **2011**, *315*, 138.
(17) Kwon, S.-H.; Kang, J.-H.; Seassal, C.; Kim, S.-K.; Regreny, P.; Lee, Y.-H.; Lieber, C. M.; Park, H.-G. Subwavelength plasmonic lasing from a semiconductor nanodisk with silver nanopan cavity. *Nano Lett.* **2010**, *10*, 3679.
(18) Costantini, D.; Greusard, L.; Bousseksou, A.; Wilde, Y. D.; Habert, B.; Marquier, F.; Greffet, J.-J.; Lelarge, F.; Decobert, J.; Duan, G.-H.; Colombelli, R. A hybrid plasmonic semiconductor laser. *Appl. Phys. Lett.* **2013**, *102*, 101106.
(19) Sundaravel, B.; Das, A. K.; Sekar, G. K.; Dev, B. N. Eptiaxial growth of silver on Br-passivated Si(111) substrates under high vacuum. *Appl. Surf. Sci.* **1999**, *137*, 11.
(20) Nason, T. C.; You, L.; Yang, G.-R.; Lu, T.-M. Growth of epitaxial Ag/Si films by the partially ionized beam deposition technique. *J. Appl. Phys.* **1991**, *69*, 773.
(21) Hua, B.; Motohisa, J.; Ding, Y.; Hara, S.; Fukui, T. Characterization of Fabry-Pérot microcavity modes in GaAs nanowires fabricated by selective-area metal organic vapor phase epitaxy. *Appl. Phys. Lett.* **2007**, *91*, 131112.
(22) Yang, L.; Motohisa, J.; Fukui, T.; Jia, L. X.; Zhang, L.; Geng, M. M.; Chen, P.; Liu, Y. L. Fabry-Pérot microcavity modes observed in the micro-photoluminescence spectra of the single nanowire with InGaAs/GaAs heterostructure. *Opt. Express* **2009**, *17*, 9337.
(23) Spiroka, D.; Arbiol, J.; Gustafsson, A.; Conesa-Boj, S.; Glas, F.; Zardo, I.; Heigoldt, M.; Gass, M. H.; Bleloch, A. L.; Estrade, S.; Kaniber, M.; Rossler, J.; Piero, F.; Morante, J. R.; Abstreiter, G.; Samuel, L.; Fontcuberta i Morral, A. Structural and optical properties of high quality zinc-blende/wurtzite GaAs nanowire heterostructures. *Phys. Rev. B* **2009**, *80*, 245325.
(24) Grilli, E.; Guzzi, M.; Zamboni, R.; Pavesi, L. High-precision determination of the temperature dependence of the fundamental energy gap in gallium arsenide. *Phys. Rev. B* **1992**, *45*, 1638.
(25) Jahn, U.; Lähnemann, J.; Pfüller, C.; Brandt, O.; Breuer, S.; Jenichen, B.; Ramsteiner, M.; Geelhaar, L.; Riechert, H. Luminescence of GaAs nanowires consisting of wurtzite and zinc-blende segments. *Phys. Rev. B* **2012**, *85*, 045323.
(26) Demichel, O.; Heiss, M.; Bleuse, J.; Mariette, H.; Fontcuberra i Morral, A. Impact of surfaces on the optical properties of GaAs nanowires. *Appl. Phys. Lett.* **2010**, *97*, 201907.
(27) Hocevar, M.; Giang, L. T. T.; Songmuang, R.; den Hertog, M.; Besombes, L.; Bleuse, J.; Niquet, Y.-M.; Pelekanos, N. T. Residual strain and piezoelectric effects in passivated GaAs/AlGaAs core-shell nanowires. *Appl. Phys. Lett.* **2013**, *102*, 191103.
(28) Bergman, D. J.; Stockman, M. I. Surface plasmon amplification by stimulated emission of radiation: quantum generation of coherent surface plasmons in nanosystems. *Phys. Rev. Lett.* **2003**, *90*, 027402.
(29) van Vugt, L. K.; Rühle, S.; Vanmaekelbergh, D. Phase-correlated nondirectional laser emission from the end facets of a ZnO nanowire. *Nano Lett.* **2006**, *6*, 2707.
(30) Yokoyama, H.; Brorson, S. D. Rate equation analysis of microcavity lasers. *J. Appl. Phys.* **1989**, *66*, 4801.
(31) Saxena, D.; Mokkapati, S.; Tan, H. H.; Jagadish, C. *Designing single GaAs nanowire lasers*. Conference on Optoelectronic and Microelectronic Materials and Devices, Melbourne, Australia, Dec. 12−14, 2012; IEEE: New York, 2012.
(32) Zhu, Z.; Brown, T. G. Full-vectorial finite-difference analysis of microstructured optical fibers. *Opt. Express* **2002**, *10*, 853.
(33) Arakawa, Y.; Sakaki, H. Multidimensional quantum well laser and temperature dependence of its threshold current. *Appl. Phys. Lett.* **1982**, *40*, 939.
(34) Aspnes, D. E.; Kelso, S. M.; Logan, R. A.; Bhat, R. Optical properties of $Al_xGa_{1-x}As$. *J. Appl. Phys.* **1986**, *60*, 754.
(35) Johnson, P. B.; Christy, R. W. Optical Constants of the Noble Metals. *Phys. Rev. B* **1972**, *6*, 4370.

DOI: 10.1021/ph5003945
ACS Photonics 2015, 2, 165−171